Simulation of Upper Tropospheric CO$_2$ From Chemistry and Transport Models

Xun Jiang[1][*], Qinbin Li[1], Mao-Chang Liang[2,3,4], Run-Lie Shia[4], Moustafa T. Chahine[1], Edward T. Olsen[1], Luke L. Chen[1], and Yuk L. Yung[4]

[1] Science Division, Jet Propulsion Laboratory, California Institute of Technology, USA

[2] Research Center for Environmental Changes, Academia Sinica, Taipei, Taiwan.

[3] Graduate Institute of Astronomy, National Central University, Jhongli, Taiwan.

[4] Division of Geological and Planetary Sciences, California Institute of Technology, Pasadena, USA.

[*] To whom all correspondence should be addressed. E-mail: xun@gps.caltech.edu

Abstract:

The Caltech/JPL two-dimensional (2-D), three-dimensional (3-D) GEOS-Chem, and 3-D MOZART-2 chemistry and transport models (CTMs), driven respectively by NCEP2, GEOS-4 and NCEP1 reanalysis data, have been used to simulate upper tropospheric CO_2 from 2000 to 2004. Model results of CO_2 mixing ratios agree well with monthly mean aircraft observations at altitudes between 8 and 13 km [*Matsueda et al*., 2002] in the tropics. The upper tropospheric CO_2 seasonal cycle phases are well captured by the CTMs. Model results have smaller seasonal cycle amplitudes in the southern hemisphere compared with those in the northern hemisphere, which are consistent with the aircraft data. Some discrepancies are evident between the model and aircraft data in the mid-latitudes, where models tend to underestimate the amplitude of CO_2 seasonal cycle. Comparison of the simulated vertical profiles of CO_2 between the different models reveals that the convection in the 3-D models is likely too weak in boreal winter and spring. Model sensitivity studies suggest that convection mass flux is important for the correct simulation of upper tropospheric CO_2.

1. Introduction

[1] The increasing level of atmospheric CO_2 has significant influence on the global climate changes [*Dickinson and Cicerone*, 1986]. It is very difficult to disentangle the contributions from different sources and sinks of atmospheric CO_2. Most inversions for the CO_2 sources and sinks are constrained by surface measurements [*Fan et al*., 1998; *Tans et al*., 1990; *Suntharalingam et al*., 2003; *Gurney et al*., 2004]. For example, the global three-dimensional (3-D) inverse modeling analysis of surface flask and oceanic CO_2 measurements by *Tans et al.* [1990] implied a significant carbon sink in the northern hemisphere (NH) terrestrial biosphere. The inversion of carbon fluxes shows sensitivity to CO_2 network configuration [*Gloor et al*., 2000; *Suntharalingam et al*., 2003]. In addition, the vertical transports in the models are also very important for the inversion. The Atmospheric Tracer Transport Model Intercomparison Project (TRANSCOM) was created to quantify the uncertainty in the atmospheric CO2 inversions from atmospheric transport [*Gurney et al*., 2003]. Some results from TRANSCOM and other models suggest that inversion results are also very sensitive to vertical transport in the tracer transport models [*Law et al*., 1996; *Fan et al*., 1998; *Gurney et al*., 2004].

[2] Previous modeling studies [*Randerson et al*., 1997; *Kawa et al*., 2004] have primarily employed surface measurements of CO_2 in their analysis. They compared the seasonal cycle and trend of surface CO_2 with their model results. The upper tropospheric CO_2 concentrations, from *in situ* aircraft measurements, usually differ by ~5 ppmv relative to the surface concentrations [*Anderson et al*., 1996; *Nakazawa et al*., 1997]. *Matsueda et al*. [2002] have been measuring CO_2 mixing ratios biweekly since April 1993 aboard commercial airlines at 8-13 km altitudes over the western Pacific from Australia to Japan. This data set offers a unique opportunity to test the ability of chemistry and transport models (CTMs) in simulating the upper tropospheric CO_2. The retrievals of CO_2 mixing ratios from the Atmospheric Infrared Sounder (AIRS), with a high precision of ~1-2 ppmv [*Chahine et al*., 2005; *Chahine et al*., 2008], can provide the global map of the middle to upper tropospheric CO_2 on a weekly basis. There is significant spatiotemporal variability in AIRS CO_2, which is supported by the *in situ*

aircraft observations. It remains a challenge for the CTMs to simulate the spatiotemporal CO_2 variability in the middle to upper troposphere. AIRS CO_2 retrievals can be used for constraining the vertical transport in CTMs in the future [*Chahine et al*., 2008].

[3] Using a two-dimensional (2-D) CTM, *Shia et al*. [2006] successfully simulated the seasonal cycle and trend of CO_2 in the upper troposphere. In this study, we will investigate instead how well global 3-D CTMs are able to simulate the seasonal cycle and trend of upper tropospheric CO_2. Surface emissions and vertical transport in CTMs are both very crucial for the correct simulation of CO_2. We will use two different boundary conditions to investigate the contribution of boundary conditions to the upper tropospheric CO_2. One is a boundary condition where the CO_2 surface mixing ratios are constructed with measurements from the GLOBALVIEW-CO_2 surface network. The other is with prescribed known CO_2 sources and sinks. To investigate the influence of vertical transport, we will compare results from GEOS-Chem and MOZART-2 with four different vertical transport schemes.

2. Models and Data

[4] The Caltech/JPL 2-D CTM [*Shia et al*., 2006], 3-D GEOS-Chem [*Suntharalingam et al*., 2004], and 3-D MOZART-2 [*Horowitz et al*., 2003] are used to simulate CO_2. The 2-D CTM has 18 latitude zones, equally spaced from pole to pole. It has 40 vertical layers, equally spaced in log scale of pressure from the surface to the upper boundary at 0.01 hPa. Transport in the model is by the stream function and the horizontal and vertical diffusivities taken from *Jiang et al*. [2004]. The stream function is derived from the National Center for Climate Prediction (NCEP) Reanalysis 2 data [*Jiang et al*., 2004]. For altitudes above 40 km where no NCEP data are available, we adopt the climatologically averaged circulation derived by *Fleming et al*. [2002]. There is a gradual merging of the two data sets between 30 and 40 km. An important feature of the 2-D CTM is its ability to reproduce the age of air in the stratosphere [*Morgan et al*., 2004].

[5] GEOS–Chem (v7.3.3) is driven by the Goddard Earth Observing System (GEOS-4)

assimilated meteorological data from the NASA Global Modeling Assimilation Office (GMAO). For computation efficiency, we regridded the GEOS-4 data into 2° (latitude) × 2.5° (longitude) in horizontal and 30 levels in vertical. It extends from the surface to about 0.01 hPa (~70 km). Advection is computed every 15 minutes with a flux-form semi-Lagrangian method [*Lin and Rood*, 1996]. Moist convection is computed using the GEOS convective, entrainment, and detrainment mass fluxes described by *Allen et al.* [1996a, 1996b]. The physics in the GEOS-4 analysis system are adopted from the National Center for Atmospheric Research (NCAR) Community Climate Model, Version 3 (CCM3) and Whole Atmosphere Community Climate Model (WACCM) with important modifications to make it suitable for data assimilation [*Bloom et al.*, 2005]. The deep convection scheme is based on *Zhang and McFarlane* [1995]. The shallow convection treatment follows *Hack* [1994]. The planetary boundary layer turbulence parameterization is from *Holtslag and Boville* [1993]. To investigate the influence of different vertical mixings on the upper tropospheric CO_2, we also force the GEOS-Chem model with the GEOS-3 reanalysis data, which employs the Relaxed Arakawa Schubert convection parameterization [*Moorthi and Suarez*, 1992].

[6] MOZART-2 is driven by the meteorological inputs every 6 hours from the NCEP Reanalysis 1 [*Kalnay et al.*, 1996]. Advection is computed every 20 minutes with a flux-form semi-Lagrangian method [*Lin and Rood*, 1996]. The horizontal resolution is 2.8° (latitude) × 2.8° (longitude) with 28 vertical levels extending up to approximately 40 km altitude [*Horowitz et al.*, 2003]. MOZART-2 is built on the framework of the Model of Atmospheric Transport and Chemistry (MATCH). MATCH includes representations of advection, convective transport, boundary layer mixing, and wet and dry deposition. Penetrative convection in the NCEP Reanalysis 1 is described by *Pan and Wu* [1994], which is based on *Arakawa and Schubert* [1974] as simplified by *Grell* [1993] with a saturated downdraft. Shallow convection from NCEP Reanalysis 1 is determined by *Tiedtke* [1983]. We also forced MOZART-2 with meteorological data from the middle atmosphere version of NCAR Community Climate Model (MACCM3), which has the same convective scheme as the GEOS-4 Reanalysis. We found the CO_2 results from MOZART-2 forced by MACCM3 meteorological fields are very close to that from

GEOS-Chem driven by GEOS-4 data, so we defer the detailed discussion to a separate study.

[7] The GLOBALVIEW-CO$_2$ mixing ratio data [*Tans et al*. 1998; *GLOBALVIEW-CO$_2$*, 2002] are used in this study as the lower boundary condition for the Caltech/JPL CTM, GEOS-Chem, and MOZART-2. For convenience, we refer this hereforth as the GLOBALVIEW-CO$_2$ boundary condition. Since the GLOBALVIEW-CO$_2$ data are limited in space, especially over ocean, we used the GLOBALVIEW-CO$_2$ to rescale the CO$_2$ mixing ratio in the surface. First, we use seasonal varying CO$_2$ source and sink flux boundary condition to drive the model. We also interpolate monthly mean GLOBALVIEW-CO$_2$ measurements to GEOS-chem resolution, which are 2° in the latitude. Then, we rescale the zonal mean CO$_2$ mixing ratio in the boundary by the monthly mean GLOBALVIEW-CO$_2$ measurements for each month and for each latitudinal band. The monthly mean GLOBALVIEW-CO$_2$ flask data are close to the CO$_2$ GLOBALVIEW-CO$_2$ boundary condition when they are co-located. We assume that all atmospheric CO$_2$ originating from the surface layer is practically chemically inert in the atmosphere considering its long lifetime. With the GLOBALVIEW-CO$_2$ boundary condition, discrepancy between model results and observations would help diagnose potential issues with model transport. However, we noticed that the GLOBALVIEW-CO$_2$ surface stations are sparse in the southern hemisphere (SH), and that the GLOBALVIEW-CO$_2$ boundary condition is also biased toward oceanic sites.

[8] In a separate simulation using GEOS-Chem, we use prescribed CO$_2$ sources and sinks as the boundary condition, as described in *Suntharalingam et al*. [2004]. The exchange of CO$_2$ between the terrestrial biosphere and atmosphere is based on net primary productivity and respiration fluxes from the Carnegie-Ames-Stanford (CASA) ecosystem model [*Randerson et al*., 1997]. Monthly mean biospheric CO$_2$ fluxes are used in the present study, for the inclusion of diurnal cycle appears to have relatively small effect on model CO$_2$ [*Suntharalingam et al*., 2004]. In a sensitivity study, we include the diurnally varying biospheric CO$_2$ fluxes [*Olsen and Randerson*, 2004] in the GEOS-Chem from Feb 2000 to Dec 2000. The effects of the diurnal cycle in biospheric CO$_2$

fluxes on the upper tropospheric CO_2 sampled at Matsueda's aircraft locations are relatively small. This is because the aircraft data are taken over the ocean in the upper troposphere, which is away from the boundary layer. Air-to-sea exchange of CO_2 is from *Takahashi et al*. [1997]. Estimates of fossil fuel emissions are from *Marland et al.* [2007]. Monthly mean biomass burning emissions of CO_2 are derived based on *Duncan et al*. [2003]. The maximum contribution for the CO_2 seasonal cycle is from the exchange between the biosphere and atmosphere. Fossil fuel emission and biomass burning also have relatively large contribution to the CO_2 in the NH. Due to the upwelling in the ocean, ocean is a source for atmospheric CO_2 in the tropics. Ocean is a sink for CO_2 in the middle to high latitudes [*Takahashi et al*., 1997]. Since there is an unbalanced CO_2 budget associated with the prescribed source and sink boundary condition [*Suntharalingam et al.*, 2003; *Suntharalingam et al.*, 2004], we constrain the restart file for the CO_2 mixing ratio in the beginning of each year by the GLOBALVIEW-CO_2 at the surface by regression. As a result, the unbalanced CO_2 budget is resolved in some degree. Discrepancies between the GEOS-Chem CO_2 simulations (driven by the same GEOS-4 reanalysis data) with the above-mentioned two boundary conditions would help identify potential issues with the surface sources and/or sinks on simulating CO_2 seasonal cycle.

[9] The details for the different model experiments are summarized in Table 1. Since Experiments A and B are forced by the same transport, GEOS-4 assimilated meteorology field, the only difference between the two experiments is the boundary conditions. Experiment A is forced by the GLOBALVIEW-CO_2 boundary condition, which is constrained by the monthly mean GLOBALVIEW-CO_2 surface flask data. Experiment B is forced by the flux boundary condition, in which we constrain the restart file for the CO_2 mixing ratio in January of each year by the GLOBALVIEW-CO_2 at the surface by regression method. Thus the main difference between the two experiments is the boundary condition from February to December in each year. Experiment A and Experiment E are forced by the same boundary conditions with different transport fields. The difference between Experiments A and E represents the difference in the transport fields. Model results will be compared with aircraft measurements from *Matsueda et al*. [2002] and GLOBALVIEW-CO_2 [*GLOBALVIEW-CO₂*, 2002] in Section 3. Aircraft CO_2

from *Matsueda et al*. [2002] are measured biweekly since April 1993 to present. The latitudinal coverage is approximately from 35°S to 35°N. The longitudinal coverage is from 135°E to 150°E. The CO_2 at 8-13 km over the western Pacific from Australia to Japan are measured. We also compared the model results with GLOBALVIEW-CO_2 aircraft measurements at Carr (40.9°N, 104.8°W) and Poker Flat (65.07°N, 147.29°W) in the auxiliary material.

3. Results

[10] To quantitatively compare the aforementioned aircraft observations and model results of CO_2, it is essential to separate trend from seasonal and semi-annual cycles in the data. For which a widely used approach is fitting data by a series of Legendre polynomials and harmonic functions [*Prinn et al.,* 2000]. We thus decompose CO_2 concentrations using the following empirical model:

$$X(t) = a + bNP_1(t/N - 1) + 1/3cN^2P_2(t/N - 1) + 1/5dN^3P_3(t/N - 1) \\ + e\cos(2\pi t) + f\sin(2\pi t) + g\cos(4\pi t) + h\sin(4\pi t) \tag{1}$$

where t is from 0 to the 2N year (whole time period); P_1, P_2, and P_3 are the first, second, and third Legendre polynomials. The coefficients a, b, c, and d are the mean value, the trend, the acceleration in the trend, and the coefficient for P_3, respectively. We add the third Legendre function to better fit the data sets. The harmonic functions are added for seasonal and semi-annual cycles. e and f are the amplitudes of the annual cycle, while g and h are the amplitudes of the semi-annual cycle. Seasonal cycle amplitude ($\sqrt{e^2 + f^2}$) for CO_2 is listed in Table 2.

[11] Figure 1 compare the aircraft observations of CO_2 averaged between 8 and 13 km (red dots) [*Matsueda et al*., 2002] and model results averaged at the same altitude range for 2000-2004. The panels are for 35°S to 35°N latitudes in 10° steps. CO_2 from all 3-D CTMs are sampled as the same location as the aircraft data. The zonal mean CO_2 from the 2-D CTM are compared with the aircraft data directly. The amplitudes of the seasonal cycle of CO_2 are smaller in the SH than those in the NH, for there is less contribution from the seasonal cycle in the vegetation photosynthesis. The green dashed line shows

results from a GEOS-Chem simulation driven by GEOS-4 data using the GLOBALVIEW-CO_2 boundary condition (Experiment A in Table 1). The orange dash-dotted line is GEOS-Chem CO_2 (driven by GEOS-4 data) with prescribed sources and sinks (Experiment B). Results from these two simulations are generally consistent, except that the CO_2 seasonal cycle is smaller in Experiment B than that in Experiment A (See Table 2). Because the transport is the same in both experiments, difference in the results may reflect deficiencies in the prescribed sources/sinks in the summer in Experiment B. In general, CO_2 concentrations from Experiment B are larger than those from Experiment A in the NH from July to October, especially at 35°N. This is consistent with a possible missing terrestrial sink hypothesis in the NH by *Tans et al*. [1990]. The GEOS-Chem CO_2 forced by the GEOS-3 meteorological fields and the GLOBALVIEW-CO_2 boundary condition (pink dotted line; Experiment C) and CO_2 from MOZART-2 (blue long dash-dotted line; Experiment E) both agrees reasonably well with the aircraft data, except some underestimations of CO_2 seasonal cycle in the NH. Experiment C includes only results for 2000-2002, as GEOS-3 data are available for only up to 2002.

[12] The agreement between the 3-D model results and aircraft data is fairly good, except at the NH mid-latitudes, where the 3-D models underestimate the amplitude of the seasonal cycle of CO_2 as seen in the aircraft data, which are consistent with results found in column-averaged CO_2 by *Yang et al.* [2007]. Similar results are found by comparing the model results to the GLOBALVIEW-CO_2 aircraft CO_2 data at Carr (40.9°N, 104.8°W) and Poker Flat (65.07°N, 147.29°W) as shown in the Figs. A1-A2 of the auxiliary material. In fact, the models all tend to underestimate the seasonal cycles of CO_2 in the middle to high latitudes.

[13] To investigate this problem, we plotted the vertical profiles of CO_2 simulated by each model at 5°N (upper panel) and 35°N (lower panel) of 2003 in Figure 2. For a fair comparison between 2-D and 3-D models, we calculate the zonal mean CO_2 from all 3-D models. In the tropics (5°N) the 3-D model results closely follow that from the 2-D model. The main advantage of the 2-D model over the 3-D models appears to be a stable numerical scheme and the flexibility to fine-tune the transport in the model. The 2-D

model has been tuned to reproduce the age of air to within the errors of the measurements in the stratosphere [see, *e.g*., Appendix A of *Morgan et al*., 2004] and to simulate CO_2 reasonably well in the upper troposphere [*Shia et al*., 2006]. In the northern mid-latitudes (35°N), all 3D models seem to underestimate the upper tropospheric CO_2 in January and April of 2003. In the later part of the paper, we will discuss the key parameter that affects the upper tropospheric CO_2 most. CO_2 simulations from MOZART-2 (Experiment E) and GEOS-Chem with GLOBALVIEW-CO_2 boundary condition (Experiment A) are forced by the same boundary condition. Thus the difference of CO_2 vertical profiles produced by Experiments A and E shows that the transport is very important for CO_2 in mid-troposphere.

[14] Raw CO_2 data from the aircraft measurements and model experiments at 35°N are shown as red dots and solid lines respectively in Figure 3. Dashed lines are the sum of all terms in the right hand side of Eq. (1), which fit well with the raw aircraft data and model results. We then detrended the data by subtracting the sum of the first three Legendre functions. The results are very close to remove a third order polynomials. The detrended aircraft data in the four years are shown as red dots in Figs. 4 and 5. Diamond and error bar are the mean and standard deviation of the detrended aircraft data for each month. Black dotted line is the sum of the annual and semi-annual cycles terms in Eq. (1), which follows well the monthly mean aircraft data (Diamonds). For comparison, we also detrended the model results using the same method. Then we averaged the detrended model CO_2 from all four years. Results are shown as color lines in Figs. 4 and 5. The phase of CO_2 seasonal cycle is well captured by the different model simulations. The seasonal cycle amplitude is larger in the NH than that in the SH, which is captured by all models. Most 3-D models underestimate the seasonal cycle amplitude in the NH.

[15] The latitudinal distribution of CO_2 seasonal cycle amplitude is shown in Fig. 6. Because of the short simulation time period in Experiment C, we do not include it in Fig. 7. All 3-D models underestimate the amplitude of CO_2 seasonal cycle in the NH mid-latitudes. The seasonal cycle amplitude of upper tropospheric CO_2 in the 2-D CTM is larger than those from the 3-D models. The amplitude of CO_2 seasonal cycle is larger in

MOZART-2 than those in GEOS-Chem. The GEOS-Chem simulation forced by the GLOBALVIEW-CO$_2$ boundary condition (Experiment A) has a larger CO$_2$ seasonal cycle than the GEOS-Chem simulation forced by surface sources and sinks (Experiment B). In Figure 5, the CO$_2$ at 35°N from Experiment B (orange line) are larger than that from Experiment A (green line) during July to October. This indicates that the biospheric CO$_2$ flux in the NH might be too strong in Experiment B. The result is consistent with possible missing terrestrial sinks in the NH suggested by *Tans et al*. [1990]. GEOS-Chem CO$_2$ (Experiments A and B) overestimate the seasonal cycle amplitude in the SH, which may be due to biases in the SH transport in GEOS-4 [*Bloom et al*., 2005]. Since there are fewer rawinsonde data in the SH compared with those in the NH, the transport in the SH is less constrained in the GEOS-4 assimilated data [*Bloom et al*., 2005].

[16] To further explore the role of different parameters for simulating CO$_2$ correctly in the upper troposphere, sensitivity studies have been conducted using the GEOS-Chem model driven by GEOS-4 reanalysis data and the GLOBALVIEW-CO$_2$ boundary condition. We first perturbed the turbulent mixing in the planetary boundary layer by 50% through increasing the turbulent mixing coefficient (Experiment F). The resulting differences between the perturbed run (Experiment F) and control run (Experiment A) at 35°N are shown in Fig. 7a. The CO$_2$ concentrations differ by less than ~0.04 ppmv at altitudes below 3.5 km, a rather small effect. We also perturbed separately the convective updraft mass flux by 20% (Experiment G). The resulting differences between the perturbed run (Experiment G) and control run (Experiment A) at 35°N are shown in Fig. 7b. The largest increase of ~0.65 ppmv in CO$_2$ is found at 6 km, which is very significant for simulating the upper tropospheric CO$_2$. Compared with the turbulent mixing in the boundary layer, the convective mass flux is more important for lifting the CO$_2$ from surfaces to the middle and upper troposphere.

[17] Accurate simulation of CO$_2$ concentrations in the upper troposphere is also imperative for deducing the inter-hemispheric transport of CO$_2$. It is generally accepted that the NH is a net CO$_2$ source and the SH (the oceans) is a net CO$_2$ sink [*IPCC*, 2001]. Previous studies [*Prather et al*. 1987; *Prinn et al*., 1992] and recent study on

interhemispheric transport of GEOS-Chem CO [*Cai et al.*, 2008] suggest that a large component of the inter-hemispheric transport occurs in the upper troposphere. Therefore, correctly modeling upper tropospheric CO_2 takes on added significance. Consider a flux inversion in which CO_2 in the NH was not efficiently transported to the upper troposphere, resulting in less transport to the SH and a lower calculated southern ocean sink. This would create artificially high CO_2 in the NH, demanding a large land sink to reconcile the model predictions with the observations. Such arguments have recently been advanced by *Stephens et al.* [2007] and *Baker* [2007].

4. Conclusions

[18] 2-D and 3-D chemistry and transport models, driven by different transport schemes, have been used to simulate the upper tropospheric CO_2 from 2000 to 2004. We also apply different boundary conditions to force the 3-D CTMs. We found that the transport schemes are very important for simulating the upper tropospheric CO_2. Model CO_2 agree generally well with the aircraft data from 35°S to 35°N. The trends of CO_2 are simulated correctly by most of the models. The phases of CO_2 seasonal cycles are also captured well by models. Similar to those in the aircraft data, model CO_2 have a smaller seasonal cycle amplitudes in the SH compared with those in the NH. However, 3-D CTMs appear to underestimate the seasonal cycle amplitude of upper tropospheric CO_2 in the NH mid-latitudes. Sensitivity studies reveal that the convective mass fluxes are very crucial for simulating the upper tropospheric CO_2. In addition to the aircraft data, global AIRS CO_2 data will become available in the near future [*Chahine et al.*, 2008]; global total column CO_2 data will be available in two years [*Crisp et al.*, 2004]. These data can be used to constrain the vertical and horizontal transport in the CTMs, resulting in more realistic models. This will give us greater confidence in deducing sources and sinks of CO_2 using a combination of global CO_2 data and inverse modeling [*Miller et al.*, 2007].

References:

Allen, D. J., R. B. Rood, A. M. Thompson, and R. D. Hidson (1996a), Three-dimensional [222]Rn calculations using assimilated data and a convective mixing algorithm, *J. Geophys. Res.*, *101*, 6871-6881.

Allen, D. J., *et al*. (1996b), Transport induced interannual variability of carbon monoxide using a chemistry and transport model, *J. Geophys. Res.*, *101*, 28655-28670.

Anderson, B. E. *et al*. (1996), Airborne observations of spatial and temporal variability of tropospheric carbon dioxide, *J. Geophys. Res.*, *101*(D1), 1985-1997.

Andres, R. J., G. Marland, I. Fung, and E. Matthews (1996), Distribution of carbon dioxide emissions from fossil fuel consumption and cement manufacture, 1950-1990, *Global Biogeochem. Cycles*, *10*, 419-429.

Arakawa, A., and W. H. Shubert (1974), Interaction of a cumulus ensemble with the large-scale environment, Part I, *J. Atmos., Sci*., *31*, 674-704.

Baker, D. F. (2007), Reassessing carbon sinks, *Science*, *316*, 1708-1709.

Bloom, S., *et al*. (2005), The Goddard Earth Observation System Data Assimilation System, GEOS DAS Version 4.0.3: Documentation and Validation, NASA TM-2005-104606, *26*, 166pp.

Cai, C., *et al*. (2008), A satellite perspective on the interhemispheric transport of pollution, *In Preparation*.

Chahine, M., *et al*., (2005), On the determination of atmospheric minor gases by the method of vanishing partial derivatives with application to CO_2, *Geophys. Res. Lett*., *32*(22), L22803.

Chahine, M., *et al*., (2008), First satellite remote sounding of the global distribution of mid-tropospheric CO_2, *In Preparation*.

Crisp, D., *et al*., (2004), The orbiting carbon observatory (OCO) mission, *Advances in Space Research*, *34*, 700-709.

Dickinson, R. E., and R. J. Cicerone (1986), Future global warming from atmospheric trace gases, *Nature, 319*(6049), 109-115.

Duncan, B. N., *et al*. (2003), Interannual and seasonal variability of biomass burning emissions constrained by satellite observations, *J. Geophys. Res.*, *108*, doi:10.1029/2002JD002378.

Fan, S., *et al*. (1998), A large terrestrial carbon sink in North America implied by atmospheric and oceanic CO_2 data and models, *Science*, *282*, 442–446.

Fleming, E. L., *et al*. (2002), Two-dimensional model simulations of the QBO in ozone and tracers in the tropical stratosphere, *J. Geophys. Res.*, *107*, doi:10.1029/2001JD001146.

GLOBALVIEW-CO_2 (2007), *Cooperative Atmospheric Data Integration Project: Carbon Dioxide* [CD-ROM], NOAA ESRL, Boulder, Colorado (Also available on Internet via anonymous FTP to ftp.cmdl.noaa.gov, Path: ccg/co2/GLOBALVIEW)

Gloor, M. (2000), Optimal sampling of the atmosphere for purpose of inverse modeling: A model study, *Global Biogeochem. Cycles*, *14*(1), 407-428.

Grell, G. A. (1993), Prognostic evaluation of assumptions used by cumulus parameterizations, *Mon. Wea. Rev.*, *121*, 764-787.

Gurney, K. R, *et al*. (2003), TransCom 3 CO2 inversion intercomparison: 1. Annual mean control results and sensitivity to transport and prior flux information, *Tellus, Ser. B, 55*, 555-579.

Gurney, K. R. *et al*. (2004), Transcom 3 inversion intercomparison: Model mean results for the estimation of seasonal carbon sources and sinks, *Global Biogeochem. Cycles*, *18*(1), GB1010.

Kalnay, E., *et al.* (1996), The NCEP/NCAR 40-year reanalysis project, *Bull. Am. Meteorol. Soc*., *77*, 437-471.

Kawa, S. R., *et al*. (2004), Global CO2 transport simulations using meteorological data from the NASA data assimilation system, *J. Geophys. Res.*, *109*, doi:10.1029/2004JD004554.

Hack, J. J. (1994), Parameterization of moist convection in the NCAR community climate model (CCM2), *J. Geophys. Res.*, *99*, 5551-5568.

Holtslag, A., and B. Boville (1993), Local versus nonlocal boundary-layer diffusion in a global climate model, *J. Clim*., *6*, 1825-1842.

Horowitz, L. W., *et al*. (2003), A global simulation of tropospheric ozone and related tracers: description and evaluation of MOZART, version 2, *J. Geophys. Res.*, *108*, doi:10.1029/2002JD002853.

IPCC (2001), *IPCC Third Accessment Report (TAR): Climate Change 2001*, Intergovernmental Panel on Climate Change.

Jiang, X. C. D. Camp, R. Shia, D. Noone, C. Walker, and Y. L. Yung (2004), Quasi-biennial oscillation and quasi-biennial oscillation-annual beat in the tropical total column ozone: A two-dimensional model simulation, *J. Geophys. Res.*, *109*, Art. No. JD004377.

Law, R., *et al*. (1996), Variations in modeled atmospheric transport of carbon dioxide and the consequences for CO_2 inversions, *Global Biogeochem. Cycles*, *10*, 783-796.

Lin, S. J., and R. B. Rood (1996), Multidimensional flux form semi-Lagrangian transport schemes, *Mon. Weather Rev.*, *124*, 2046-2070.

Marland, G., T. A. Boden, and R. J. Andres, Global, Regional, and National CO_2 Emissions. In *Trends: A Compendium of Data on Global Change. Carbon Dioxide Information Analysis Center*, Oak Ridge National Laboratory, U.S. Department of Energy, (Oak Ridge, TN, 2007).

Matsueda, H., H. Y. Inoue, and M. Ishii (2002), Aircraft observation of carbon dioxide at 8-13 km altitude over the western Pacific from 1993 to 1999, *Tellus*, *54B*(1), 1-21. The data are available at http://gaw.kishou.go.jp/wdcgg.html

Miller, C. E., *et al*. (2007), Precision requirements for space-based Xco$_2$ data, *J. Geophys. Res.*, *112*, doi:10.1029/2006JD007659.

Moorthi, S., and M. J. Suarez (1992), Relaxed Arakawa-Schubert – A parameterization of moist convection for general circulation models, *Mon. Wea. Rev.*, *120*(6), 978-1002.

Morgan, C. G., *et al*. (2004), Isotopic fractionation of nitrous oxide in the stratosphere: Comparison between model and observations, *J. Geophys. Res.*, *109*, D04305.

Nakazawa, T., *et al*. (1997), Aircraft measurements of the concentrations of CO_2, CH_4, N_2O, and CO and the carbon and oxygen isotopic ratios of CO_2 in the troposphere over Russia, *J. Geophys. Res.*, *102*, 3843-3859.

Olsen, S. C., and J. T. Randreson (2004), Differences between surface and column atmospheric CO2 and implications for carbon cycle research, *J. Geophys. Res.*, *109*, doi:10.1029/2003JD003968.

Pan, H. L., and W. S. Wu (1994), Implementing a mass flux convection parameterization package for the NMC medium-range forecast model, *NMC office note*, No. 409, 40pp.

Prather, M., *et al*. (1987), Chemistry of the global troposphere: Fluorocarbons as tracers of air motion, *J. Geophys. Res.*, *92*, 6579-6613.

Prinn, R. G., *et al*. (1992), Global average concentration and trend for hydroxyl radicals deduced from ALE/GAGE trichloroethane (methylchloroform) data for 1978-1990, *J. Geophys. Res.*, *97*, 2445-2461.

Prinn, R. G., *et al*. (2000), A history of chemically and radiatively important gases in air deduced from ALE/GAGE/AGAGE, *J. Geophys. Res.*, *105*, 17751-17792.

Randerson, J. T., *et al*. (1997), The contribution of terrestrial sources and sinks to trends in the seasonal cycle of atmospheric carbon dioxide, *Global Biogeochem. Cycles*, *11*, 535-560.

Shia, R., M. Liang, C. E. Miller, and Y. L. Yung (2006), CO_2 in the upper troposphere: influence of stratosphere-troposphere exchange, *Geophys. Res. Lett., 33*, doi:10.1029/2006GL026141.

Stephens, B. B, *et al*. (2007), Weak northern and strong tropical land carbon uptake from vertical profiles of atmospheric CO_2, *Science*, *316*, 1732-1735.

Suntharalingam, P., *et al*. (2003), Estimating the distribution of terrestrial CO2 sources and sinks from atmospheric measurements: sensitivity to configuration of the observation network, *J. Geophys. Res.*, *108*, doi:10.1029/2002JD002207.

Suntharalingam, P., *et al*. (2004), Improved quantification of Chinese carbon fluxes using CO2/CO correlations in Asian outflow, *J. Geophys. Res.*, *109*(D18), doi:10.1029/2003JD004362.

Takahashi, T., *et al*. (1997), Global air-sea flux of CO2: An estimate based on measurements of sea-air pCO2 difference, *Proc. Natl. Acad. Sci. U. S. A.*, *94*, 8929.

Tans, P. P., I. Y. Fung, and T. Takahashi (1990), Observational constraints on the global atmospheric CO_2 budget, *Science*, *247* (4949): 1431-1438.

Tans, P.P., *et al*. (Eds.) (1998), Carbon Cycle, in *Climate Monitoring and Diagnostics Laboratory No. 24 Summary Report 1996-1997*, edited by D.J. Hoffmann *et al*., chap. 2, pp. 30-51, NOAA Environ. Res. Lab., Boulder Colo. (Data available from http://www.cmdl.noaa.gov/)

Tiedtke, M. (1983), The sensitivity of the time-mean large-scale flow to cumulus convection in the ECMWF model, *ECMWF workshop on convection in large-scale models*, Reading, England, pp. 297-316.

Yang, Z. *et al*. (2007), New constraints on northern hemisphere growing season net flux, *Geophys. Res. Lett., 34*, doi:10.1029/2007GL029742.

Zhang, G. J., and N. A. McFarlane (1995), Sensitivity of climate simulations to the parameterization of cumulus convection in the Canadian climate centre general circulation model, *Atmos. Ocean*, *33*, 407-446.

Figure Captions:

Figure 1: Aircraft observations between 8 km and 13 km (red dots) [*Matsueda et al.*, 2002] and modeled CO_2 mixing ratios averaged at the same layer from 2000 to 2004. The panels are for 35°S, 25°S, 15°S, 5°S, 5°N, 15°N, 25°N, and 35°N, respectively. The CO_2 mixing ratios from the GEOS-Chem model (Experiments A, B, and C) are shown by the green dashed, orange dash-dotted, and pink dotted lines, respectively. The CO_2 mixing ratios from the Caltech-JPL 2-D model (Experiment D) are shown by purple solid lines. The CO_2 mixing ratios from MOZART-2 (Experiment E) are shown by the blue long dash-dotted lines.

Figure 2: Vertical profiles of CO_2 in January, April, July, and October 2003. Colors are the same as in Figure 1. Upper panel: Latitude = 5°N. Lower panel: Latitude = 35°N.

Figure 3: CO_2 from aircraft and models at 35°N. Red dots are aircraft observations. Solid lines are model results. Colors are the same as in Figure 1. Dashed lines are the fit to the CO_2 (see text).

Figure 4: CO_2 seasonal cycles from detrended aircraft (Red dots) and detrended model results (Color lines) at 25°S, 15°S, and 5°S. Trends are determined by the sum of the first three legendre polynomials. Diamond and the error bar are the mean and standard deviation of the detrended aircraft data within each month. Black dotted line is the sum of the annual and semi-annual cycles terms in Eq. (1).

Figure 5: CO_2 seasonal cycles from detrended aircraft (Red dots) and detrended model results (Color lines) at 5°N, 15°N, 25°N, and 35°N. Trends are determined by the sum of the first three legendre polynomials. Diamond and error bar are the mean and standard deviation of the detrended aircraft data within each month. Black dotted line is the sum of the annual and semi-annual cycles terms in Eq. (1).

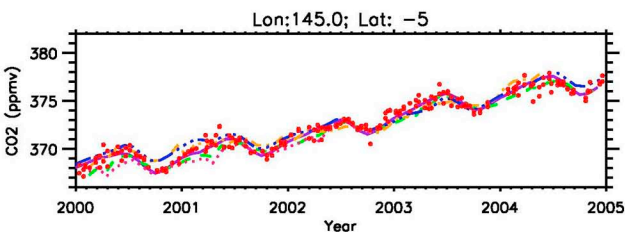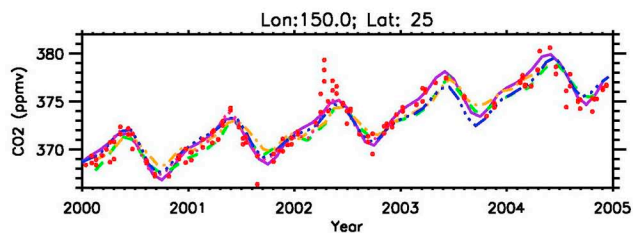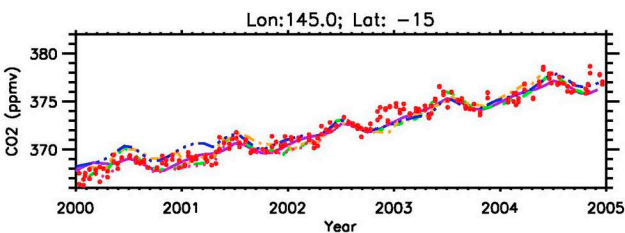Figure 6: Latitudinal distribution of CO_2 seasonal cycle amplitude.
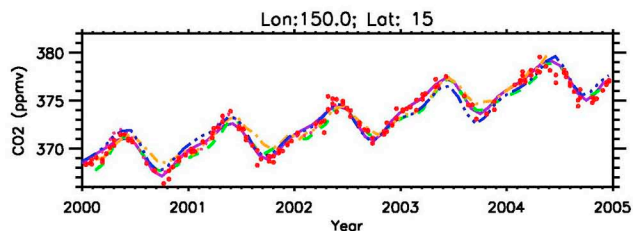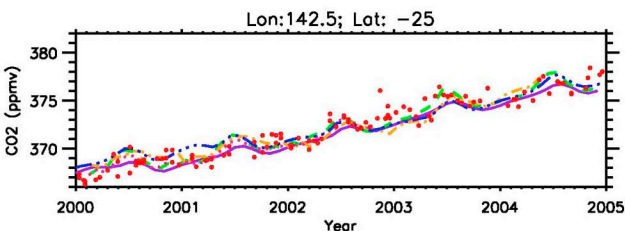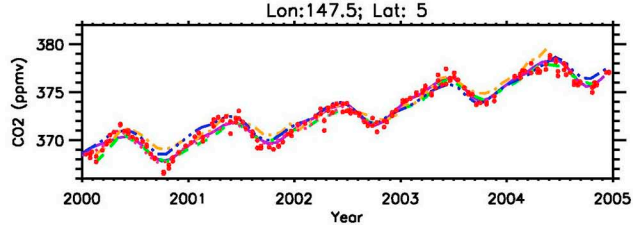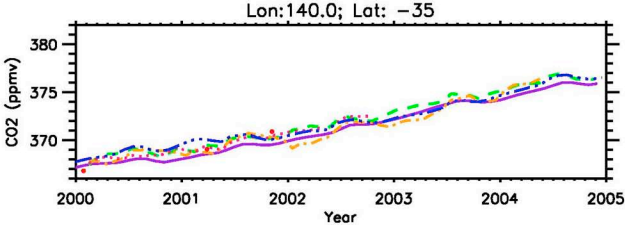
Figure 7: (a) CO_2 difference between the enhanced turbulence mixing in the planetary boundary layer simulation and control experiment at 35°N. (b) CO_2 difference between the enhanced convective updraft mass flux simulation and control experiment at 35°N.
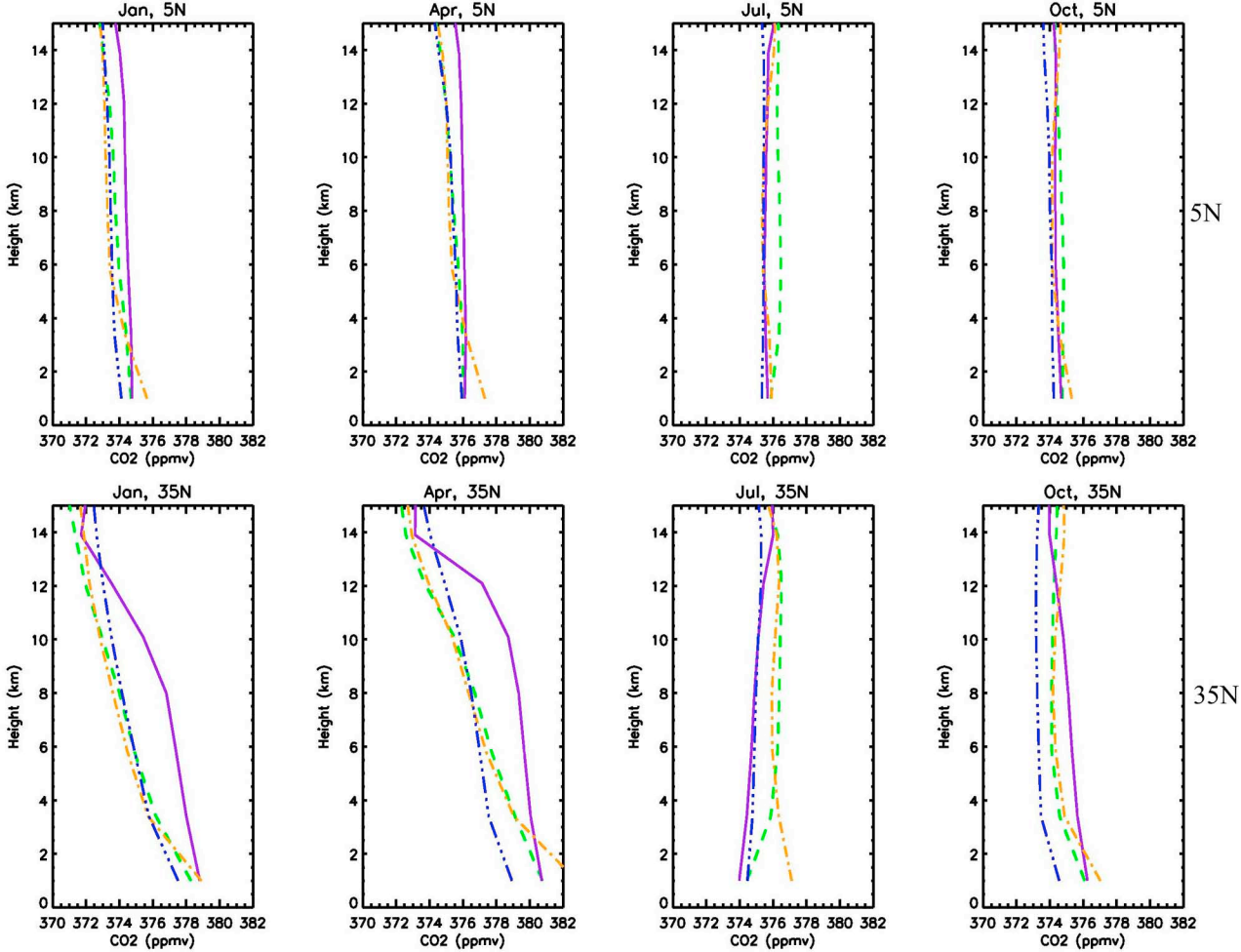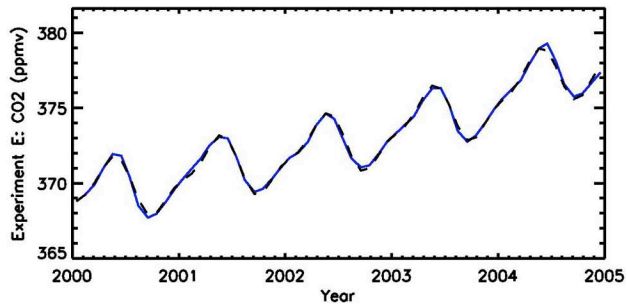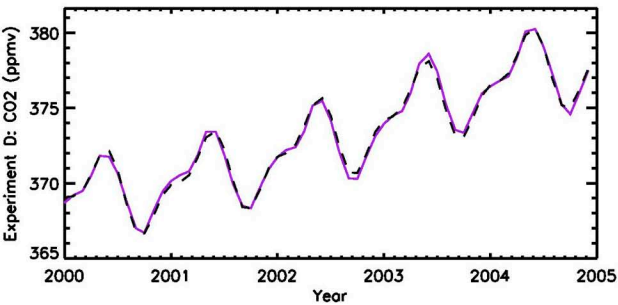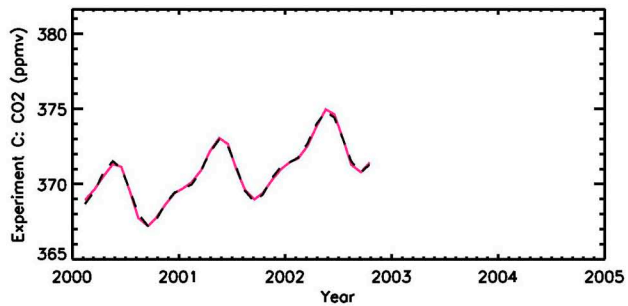
Table 1: Description of Model Experiments.

	Model	Transport	Boundary Condition	Model Change
Experiment A	3-D GEOS-Chem	GEOS-4	GLOBALVIEW-CO_2	
Experiment B	3-D GEOS-Chem	GEOS-4	CO_2 sources and sinks	
Experiment C	3-D GEOS-Chem	GEOS-3	GLOBALVIEW-CO_2	
Experiment D	2-D Caltech/JPL CTM	NCEP2 and UKMO	GLOBALVIEW-CO_2	
Experiment E	3-D MOZART2	NCEP1	GLOBALVIEW-CO_2	
Experiment F	3-D GEOS-Chem	GEOS-4	GLOBALVIEW-CO_2	Increase turbulence mixing in the PBL by 50%
Experiment G	3-D GEOS-Chem	GEOS-4	GLOBALVIEW-CO_2	Increase the convective updraft mass flux by 20%

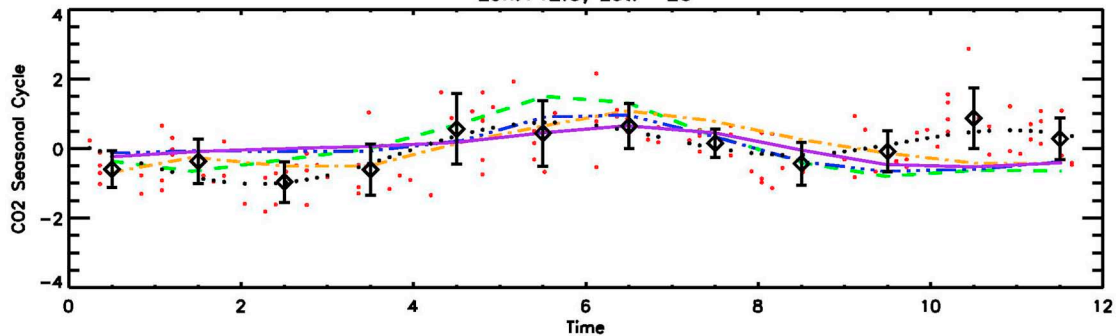Table 2: Seasonal Cycle Amplitude of CO_2 From Matsueda Aircraft data and Model Simulations.

	Seasonal Cycle Amplitude (ppmv)							
Aircraft		0.38±0.14	0.38±0.08	0.90±0.08	1.61±0.08	2.05±0.09	2.47±0.17	2.48±0.3
Experiment A	0.28±0.06	0.95±0.08	1.03±0.1	0.74±0.08	1.21±0.07	1.64±0.06	1.61±0.06	1.51±0.07
Experiment B	0.57±0.08	0.7±0.09	0.74±0.1	0.57±0.1	1.17±0.07	1.5±0.07	1.3±0.06	1.32±0.07
Experiment C	0.1±0.08	0.64±0.07	0.83±0.1	0.52±0.1	1.24±0.11	1.98±0.09	2.06±0.06	1.87±0.05
Experiment D	0.21±0.05	0.49±0.07	0.66±0.08	1.06±0.07	1.44±0.07	1.94±0.07	2.33±0.07	2.36±0.08
Experiment E	0.28±0.05	0.58±0.05	0.64±0.06	0.77±0.06	1.30±0.05	1.88±0.06	1.90±0.07	1.88±0.06

Lon:140.0; Lat: −35   Lon:147.5; Lat: 5
Lon:142.5; Lat: −25   Lon:150.0; Lat: 15
Lon:145.0; Lat: −15   Lon:150.0; Lat: 25
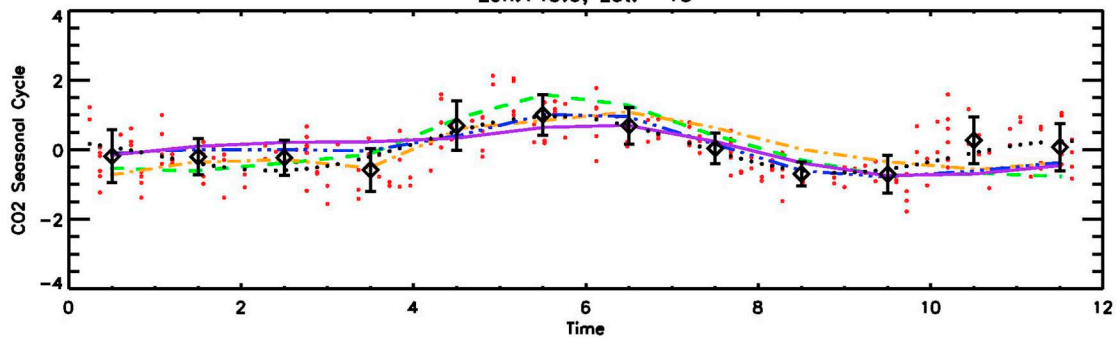Lon:145.0; Lat: −5   Lon:152.5; Lat: 35

- - - A   · — · B   ········· C   —— D   ·· — ·· E
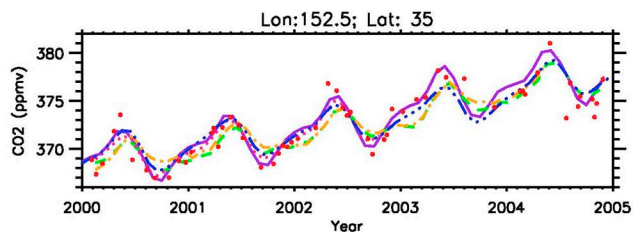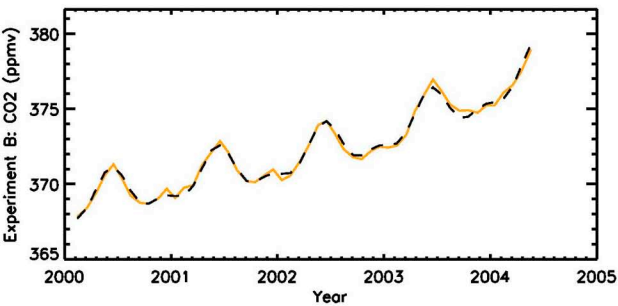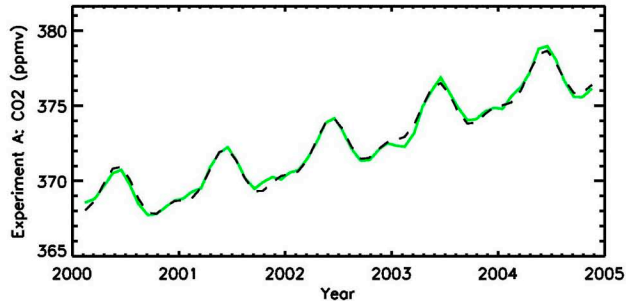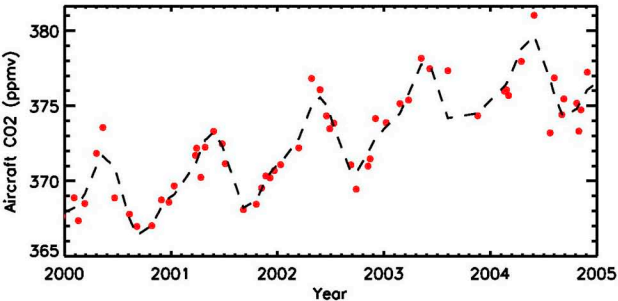
Lon:142.5; Lat: −25

Lon:145.0; Lat: −15

Lon:145.0; Lat: −5

A   B   D   E

(a)
(b)